Optically Modulated Electrokinetic Manipulation and Concentration of Colloidal Particles near an Electrode Surface

Aloke Kumar,[†] Jae-Sung Kwon,[†] Stuart J. Williams,[▼] Nicolas G. Green,[‡] Nung Kwan Yip,[§] and Steven T. Wereley*,[†]

[†]Birck Nanotechnology Center and School of Mechanical Engineering, Purdue University, West Lafayette, Indiana 47907, [▼]School of Mechanical Engineering, University of Louisville, Louisville, Kentucky 40292, [‡]School of Electronics and Computer Science, University of Southampton, Highfield, Southampton SO17 1BJ, United Kingdom, and [§]Department of Mathematics, Purdue University, West Lafayette, Indiana 47907

We study a recently demonstrated AC electrokinetic technique for manipulation and concentration of colloidal particles on an electrode surface. The technique uses indium tin oxide (ITO)-based parallel-plate electrodes on which highly localized infrared (1064 nm) laser illumination is shone. We show that the highly localized laser illumination leads to a highly nonuniform heating of the electrode substrate, which in turn drives an electrothermal microvortex resulting in a rapid transport of particles toward the illuminated site. Hundreds of polystyrene particles, with diameters ranging from 2.0 to 0.1 μm, suspended in a low conductivity solution (2.0 mS/m) could be aggregated at selected locations on the electrode by activating the laser illumination at suitable AC frequencies. Subsequent deactivation of the laser illumination causes the particles to scatter, and we explore this dynamical behavior for 1.0 μm particles using Delaunay tessellations and high-speed videography. We establish that drag from the electrothermal microvortex acts against a repulsive force, which decreases with increasing AC frequency, to create stable particle clusters. Moreover, experimentally we show that this particle capturing technique can be characterized by a critical frequency: a frequency at which the captured colloidal particle cluster becomes unstable and particles are carried away into the bulk by the electrothermal microvortex. This critical frequency increases with decreasing particle diameter for similar particles. For 0.1 μm particles, comparison of aggregation at different AC frequencies is achieved by the comparison of fluorescent intensity profiles of the aggregations.

1. Introduction

The need and ability to manipulate and assemble colloidal micro- and nanoparticles is highly relevant for a broad range of microengineering applications. The diversity of AC electrokinetic phenomena has caused it to acquire a prominent position in the various technological tools that exist nowadays for the manipulation of colloidal particles.[1,2] While complex electrode geometries can be employed for such applications,[3,4] the assembly of micro- and nanoparticles is also possible with an even simpler parallel uniform electrode configuration.[5−12] Electrokinetic colloidal aggregation within this electrode configuration has found numerous applications,[13,14] including concentration of nanoparticles[6,15] and biological cells.[16,17] In addition, optical modulation of colloidal assemblies in such a simple system has been attempted either through the use of a broad ultraviolet (UV) illumination source[18] or through the use of focused laser beam (532 nm) that has the capability to scan various spatial patterns.[19]

Recently, Williams et al.[20] introduced the technique of rapid electrokinetic patterning (REP), a noninvasive optically modulated technique for the manipulation of micro- and nanoparticles on an electrode surface. This technique employed a simple parallel uniform electrode setup with an applied AC electric field. The

*To whom correspondence should be addressed. E-mail: wereley@purdue.edu.

(1) Morgan, H.; Green, N. G. *AC electrokinetics: colloids and nanoparticles*; Research Studies Press: Philadelphia, PA, 2003; p xvi, 324 pp.

(2) Williams, S. J. AC Dielectrophoresis Lab-on-Chip Devices. In *Encyclopedia of Microfluidics and Nanofluidics*; Li, D., Ed.; Springer: New York, 2008; Vol. 1.

(3) Morgan, H.; Green, N. G. Dielectrophoresis. In *Encyclopedia of Microfluidics and Nanofluidics*; Li, D., Ed.; Springer: New York, 2008; Vol. 1.

(4) Williams, S. J. Dielectrophoretic Motion of Particles and Cells. In *Encyclopedia of Microfluidics and Nanofluidics*; Li, D., Ed.; Springer: New York, 2008; Vol. 1.

(5) Bohmer, M. In situ observation of 2-dimensional clustering during electrophoretic deposition. *Langmuir* 1996, 12 (24), 5747−5750.

(6) Giersig, M.; Mulvaney, P. Formation of ordered 2-dimensional gold colloid lattices by electrophoretic deposition. *J. Phys. Chem.* 1993, 97 (24), 6334−6336.

(7) Giner, V.; Sancho, M.; Lee, R. S.; Martinez, G.; Pethig, R. Transverse dipolar chaining in binary suspensions induced by rf fields. *J. Phys. D: Appl. Phys.* 1999, 32 (10), 1182−1186.

(8) Gong, T. Y.; Wu, D. T.; Marr, D. W. M. Two-dimensional electrohydrodynamically induced colloidal phases. *Langmuir* 2002, 18 (26), 10064−10067.

(9) Richetti, P.; Prost, J.; Barois, P. Two-dimensional aggregation and crystallization of a colloidal suspension of latex spheres. *J. Phys. Lett.* 1984, 45 (23), 1137−1143.

(10) Trau, M.; Saville, D. A.; Aksay, I. A. Field-induced layering of colloidal crystals. *Science* 1996, 272 (5262), 706−709.

(11) Trau, M.; Saville, D. A.; Aksay, I. A. Assembly of colloidal crystals at electrode interfaces. *Langmuir* 1997, 13 (24), 6375−6381.

(12) Yeh, S. R.; Seul, M.; Shraiman, B. I. Assembly of ordered colloidal aggregates by electric-field-induced fluid flow. *Nature* 1997, 386 (6620), 57−59.

(13) Velev, O. D.; Jede, T. A.; Lobo, R. F.; Lenhoff, A. M. Porous silica via colloidal crystallization. *Nature* 1997, 389 (6650), 447−448.

(14) Whitesides, G. M.; Grzybowski, B. Self-assembly at all scales. *Science* 2002, 295 (5564), 2418−2421.

(15) Teranishi, T.; Hosoe, M.; Tanaka, T.; Miyake, M. Size control of monodispersed Pt nanoparticles and their 2D organization by electrophoretic deposition. *J. Phys. Chem. B* 1999, 103 (19), 3818−3827.

(16) Bhatt, K. H.; Grego, S.; Velev, O. D. An AC electrokinetic technique for collection and concentration of particles and cells on patterned electrodes. *Langmuir* 2005, 21 (14), 6603−6612.

(17) Poortinga, A. T.; Bos, R.; Busscher, H. J. Controlled electrophoretic deposition of bacteria to surfaces for the design of biofilms. *Biotechnol. Bioeng.* 2000, 67 (1), 117−120.

(18) Hayward, R. C.; Saville, D. A.; Aksay, I. A. Electrophoretic assembly of colloidal crystals with optically tunable micropatterns. *Nature* 2000, 404 (6773), 56−59.

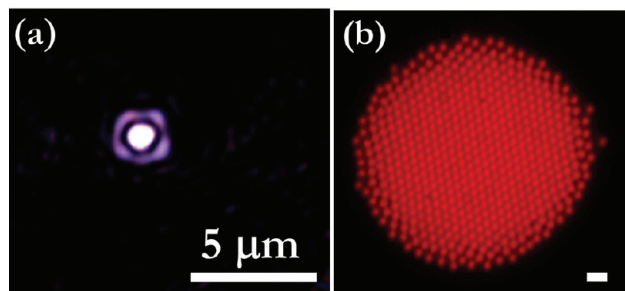(19) Gong, T. Y.; Marr, D. W. M. Photon-directed colloidal crystallization. *Appl. Phys. Lett.* 2004, 85 (17), 3760−3762.

(20) Williams, S. J.; Kumar, A.; Wereley, S. T. Electrokinetic patterning of colloidal particles with optical landscapes. *Lab Chip* 2008, 8 (11), 1879−1882.
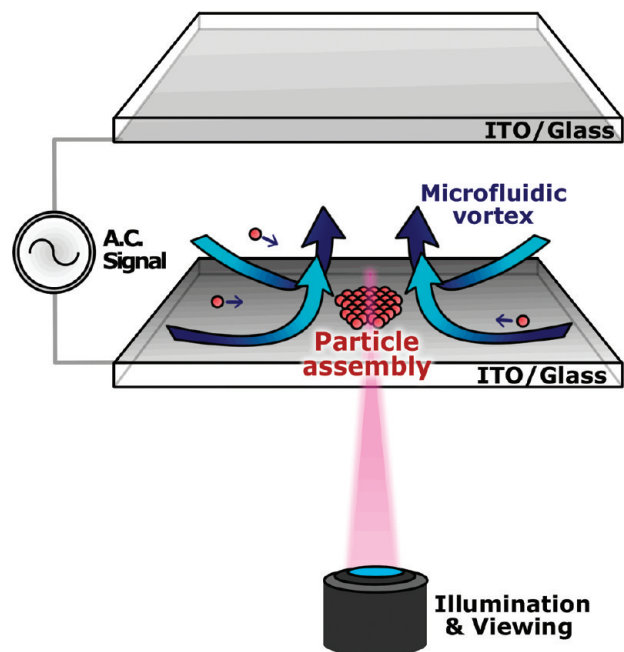
Figure 1. Illustration of particle accumulation using the REP technique. An electrothermal microfluidic vortex causes rapid particle transport to the illuminated region on the electrode surface. The particle cluster is held close to the electrode surface and can be translated to a desired location simply by changing the spatial location of the illumination.

Figure 2. (a) Optical landscape, resulting from tightly focusing the 1064 nm laser, on an electrode surface. The scope of the present investigation emphasizes on this simple optical landscape geometry. (b) Large REP cluster of red-fluorescent 1.0 μm particles resulting from such an optical landscape. Note that the REP cluster can be several times bigger than the size of the optical landscape.

optical landscape was provided by holograms generated from an infrared (1064 nm) laser (Figure 1). They showed that, in a low AC frequency regime (< 200 kHz), particles could be dynamically configured into various shapes by the use of holograms generated from a spatial light modulator (SLM). REP is primarily an electrokinetic technique, where optically modulated electrokinetics serve to rapidly transport particles to the illuminated locations on the electrode surface,[21] leading to particle aggregation (Figures 1 and 2). Aggregation in REP is localized to the region of illumination and such a local nature allows for dynamic manipulation by REP as clusters can be translated on the electrode surface by either moving the stage or 'blinking' the illumination from one location to the next (see video).[22] Initially, Williams et al.[20] demonstrated successful manipulation of particles ranging in size from 300 nm to 3.0 μm. However, now REP has demonstrated an ability to concentrate polystyrene nanoparticles as small as 50 nm using relatively low optical powers and electrical voltages compared to optical traps and dielectrophoresis, respectively.[23,24] The dynamic nature and versatility of REP makes the technique a promising noninvasive manipulation tool.

Electrothermal hydrodynamic drag and electrokinetic mechanisms such as dipole−dipole repulsive forces drive REP. In order to explore the mechanisms that cause a stable particle cluster in REP, it is necessary to understand the temperature gradients that drive the electrothermal flow and also the role of other contributing electrokinetic forces on experimental parameters. In their investigation, Williams et al.[20] suggested the role of electrothermal flows in the rapid transport of particles to the illuminated regions on the electrode. Kumar et al.[25] performed detailed fluid flow visualization experiments to characterize fluid flow and found that fluid flow in a REP platform resembled a "sink-type" flow in a transverse plane close to an electrode surface, which transports particles toward an illuminated site. The "sink-type" flow near the electrode is caused by a three-dimensional toroidal fluid flow that extends between the two electrodes. While Kumar et al.[25] found agreement with the theory of electrothermal flows, the optically induced temperature (T) profile has not been determined yet. The temperature field would determine the magnitude of electrothermal flow field and hence the drag force on the particles. While the temperature profile is yet to be determined, other forces in a REP aggregation are neither fully understood nor have they been properly quantified. Forces other than electrothermal flows are expected to have a complex dependence on the electric field, and that dependence needs to be quantified so that a comprehensive understanding of the REP phenomenon can be achieved.

In this work, we expand on the initial investigation of REP and attempt to understand the roles of the laser illumination and electric field. We show that the laser illumination gives rise to a localized temperature field. The temperature field created by the infrared illumination is studied using laser induced fluorescence (LIF) thermometry. We show that very high temperature gradients are created by laser heating of the ITO substrate. We also show for a low conductivity medium (2.0 mS/m) the fluid drag due to the electrothermal microvortex is the dominant force that acts against repulsion between the colloidal particles. By studying dynamical behavior of REP aggregations of 1.0 μm polystyrene particles with high-speed videography, we were able to quantify the dependence of this net repulsive force on the electric field. This repulsive force decreases with AC frequency, suggesting the presence of a relaxation mechanism, which previously has not been explored in the context of particle aggregation in such a system. Moreover, we demonstrate experimentally that, as a consequence of the toroidal electrothermal microvortex, REP is characterized by the existence of a critical frequency. We also show that, for similar particles (carboxylate-modified polystyrene particles), this critical frequency is dependent on particle diameter.

(21) Williams, S. J.; Kumar, A.; Green, N. G.; Wereley, S. T. Optically induced electrokinetic concentration and sorting of colloids. *J. Micromech. Microeng.* **2010**, 20.

(22) Williams, S. J.; Kumar, A.; Wereley, S. T. Optically induced electrokinetic patterning and manipulation of particles. http://hdl.handle.net/1813/11399.

(23) Kumar, A.; Kwon, J.-S.; Williams, S. J.; Wereley, S. T. A novel optically driven electrokinetic technique for manipulating nanoparticles. *Proc. SPIE* **2009**, 74000V, DOI:10.1117/12.826932.

(24) Williams, S. J.; Kumar, A.; Green, N. G.; Wereley, S. T. A simple, optically induced electrokinetic method to concentrate and pattern nanoparticles. *Nanoscale* **2009**, *1*, 133−137.

(25) Kumar, A.; Williams, S. J.; Wereley, S. T. Experiments on opto-electrically generated microfluidic vortices. *Microfluid. Nanofluid.* **2009**, *6* (5), 637−646.

2. Materials and Methods

A microfluidic chip in conjunction with an optical system capable of producing highly focused infrared illumination (1064 nm) serves as the primary experimental setup. Subsequently, different aspects of the REP process are studied with techniques such as LIF thermometry and Delaunay triangulation. The experimental methods adopted in this investigation are explained in detail in the subsections that follow.

Chip Preparation. The microfluidic chip consists of a microfluidic chamber sandwiched between two parallel-plate electrodes. An indium tin oxide (ITO)-coated glass coverslip (SPI Supplies Inc., PA), 170 μm thick, was used for the bottom electrode, while the top electrode was made either from sputtered gold and chrome (Au 150 nm/Cr 50 nm) or from an ITO-coated glass substrate. The microfluidic chamber had a height of $\sim$50 μm, and it was constructed from a spacer material with millimeter sized channels. The experimental area was far from channel sidewalls to avoid any wall-based distortion of the local electric field. An AC signal was applied to the parallel-plate electrodes, resulting in a uniform electric field in the experimental area. For the chip geometry described above, REP typically requires an AC voltage, V, of less than 20 V_{pp} (volts peak-to-peak) and an AC frequency, f, of less than 200 kHz.

Prior to experimentation, the microfluidic channel was filled with an aqueous solution of potassium chloride (KCl) of desired conductivity and left for about 10 h. Subsequently, the channel was purged of this solution, and the prepared sample solution was injected into the channel manually.

Illumination System. An inverted Nikon TE2000U microscope equipped with Nikon objective lenses was used for visualization. A focused laser beam with a wavelength of 1064 nm from a Nd:YVO$_4$ laser served as the source of the optical landscape for REP (Figure 2a). The microscope objective lens served both to focus the laser and for viewing the fluorescent polystyrene beads. Unlike the study of Williams et al.,[20] holographic optical landscapes are not required in the present investigation. Only a simple focused laser spot served as the optical landscape. Laser power values (P) stated in the text refer to the total laser power impinging the back focal plane of the microscope objective lens. For viewing of beads, an epifluorescent filter cube (Nikon TRITC HYQ) was employed, and the fluorescent excitation was provided by a 120 W lamp (X-cite 120, Exfo, Quebec, Canada).

Particle Preparation. Red fluorescent carboxylate-modified polystyrene particles (Invitrogen, MD) of four different sizes (2.0, 1.0, 0.5, and 0.1 μm) were utilized for the purpose of the present investigation. Aqueous potassium chloride (KCl) solutions of conductivity (σ = 2 mS/m) were prepared, and finally individual dilute particle solutions for bead sizes 0.5–2.0 μm were prepared by mixing 50 μL of the 2% solids particle solution with 10 mL of the KCL solution of desired conductivity. The solution conductivity values contained herein refer to the measured conductivity of the aqueous KCl solution prior to mixing.

For the nanoparticles (0.1 μm red fluorescent carboxylate-modified polystyrene particles), a dilute sample was prepared by mixing 100 μL of a 2% solids particle solution with 10 mL of an aqueous solution of potassium chloride (KCl) with conductivity, σ, of 2 mS/m. A slightly higher concentration of the nanoparticles was used to overcome the reduced fluorescence at these length scales. These particles due to their near unity density ($\sim$1.05 g/mL) can be considered to be neutrally buoyant.

Video Microscopy. Video microscopy was employed to observe the behavior of the particles under the various experimental conditions. Two different primary cameras were employed depending on the type of experiment being conducted. For high-speed video microscopy, the HotShot 512 (NAC, CA) camera was utilized. The camera is a digital high-speed video system with a maximum resolution of 1280 × 1024 pixels and a pixel pitch of 16 μm × 16 μm. The HotShot was used to acquire images at 250 frames per second (fps). For other cases including visualization of
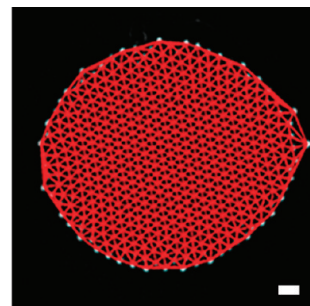
Figure 3. Delaunay tesselation of the particle aggregation in Figure 2b. The Delaunay tesselation is used to compute the ensemble averaged interparticle distance in a REP cluster. The scale bar in the image represents 5 μm.

the nanoparticles, a camera with high quantum efficiency and low read-out noise was used (PCO.1600, Cooke Corporation, MI). The camera has a maximum resolution of 1600 × 1200 pixels at a 7.4 μm × 7.4 μm pixel pitch. A Nikon 100× oil-immersion lens (1.3 numerical aperture, NA, and 0.16 mm working distance) was used for the study of all particle sizes.

For 1.0 μm particles, the study of REP clustering is initialized by focusing the infrared laser through a Nikon 100× objective lens on the bottom ITO surface and creating a stable REP aggregation. Subsequently, each particle center in the aggregation is identified. Particle centers in the acquired images were determined using a MATLAB adaptation of the IDL particle tracking software developed by Grier, Crocker, and Weeks. The adaptation by Blair and Duffresne is freely available for public use.[26] Based on particle locations, the REP clustering is analyzed by means of Delaunay triangulation. These methods have been widely applied to the analysis of the packing structure of particles, as they can provide detailed information such as the distributions of particles and surface area.[27,28] For a particle aggregation, a Voronoi diagram defines a partitioning of space where each particle is assigned a Voronoi cell corresponding to the region of space closest to a given particle and the Voronoi cells describe the arrangement of all the neighbors of the particle. Delaunay triangulation is related to the Voronoi diagram through the principle of duality, and each triangle in a Delaunay mesh is useful in quantifying the properties related to the proximity of particles. For the analysis performed here, the particle centers serve as vertices of the Delaunay triangles and the triangulation itself is achieved through the implementation of QHULL[29] (Figure 3).

We apply these two methods to observe how particles are packed in REP clusters. The Delaunay mesh is used to calculate the nondimensionalized ensemble averaged interparticle distance, which is defined as

$$\gamma = \frac{1}{a} \frac{\sum_i l_i}{n} \tag{1}$$

where a denotes the particle diameter, l_i is the length of the Delaunay triangle edges, and n is the total number of edges.

LIF Thermometry. LIF thermometry is a method for performing nonintrusive temperature measurements inside a volume of water. In LIF thermometry, a temperature sensitive dye such as Rhodamine B (RhB) is used, whose fluorescent emission depends on the temperature of the liquid. For LIF thermometry

(26) Blair, D.; Dufresne, E. The Matlab Particle Tracking Code Repository.
(27) Poupon, A. Voronoi and Voronoi-related tessellations in studies of protein structure and interaction. *Curr. Opin. Struct. Biol.* **2004**, *14* (2), 233−241.
(28) Wriggers, W.; Milligan, R. A.; McCammon, J. A. Situs: A package for docking crystal structures into low-resolution maps from electron microscopy. *J. Struct. Biol.* **1999**, *125* (2−3), 185−195.
(29) Barber, C. B.; Dobkin, D. P.; Huhdanpaa, H. The Quickhull algorithm for convex hulls. *ACM Trans. Math. Software* **1996**, *22* (4), 469−483.

experiments, the laser is used to illuminate the bottom ITO surface in the absence of any applied electric field and subsequently the fluorescence emission is recorded. Detailed discussion of the theory and application of LIF thermometry is available elsewhere.[30] A 40× water-immersion objective lens (0.8 NA, 2.0 mm working distance) was used for focusing the laser and for viewing for LIF thermometry experiments.

3. Results

On the simultaneous application of a focused laser illumination (Figure 2a) on the electrode surface and an AC electric field, rapid fluid transport occurs toward the center of laser illumination, and at a suitable AC frequency a cluster of particles, localized to the region of illumination, forms on the electrode surface. Figure 2b depicts a large REP cluster, composed of an aggregation of hundreds of 1 μm polystyrene particles, created by focusing the laser spot on the electrode surface. REP-based aggregation for neutrally buoyant particles such as polystyrene particles employed in this work can occur at either electrode surface. For consistency, all results included in this work were obtained on the bottom ITO coverslip.

A local REP aggregation is initiated only by the simultaneous presence of both the laser illumination and the electric field. To verify this, we initially activated the laser illumination in the absence of an electric field but no aggregation could be observed. Subsequently, the laser illumination was deactivated and only the electric field was activated. When the applied AC frequency was below 1 kHz, isolated particles aggregated to form "global" clusters, even in the absence of any laser illumination. These clusters are "global" in the sense they can occur anywhere on the electrode surface. However, for $f \geq 2$ kHz, the clusters again disintegrate into isolated particles. Such a phenomenon has also been observed before by Nadal et al.,[31] who used the term "contact frequency" to describe this behavior. Specifically, "contact frequency" was the AC frequency above which particles were separated from nearest neighbors by several particle radii. Thus, above the "contact frequency", the sole application of an AC electric field also does not lead to particle aggregation.

Thus, we can see that REP is an opto-electric technique, where the laser illumination and electric field act synergistically to create an aggregation of particles. Optical illumination, when it can create temperature gradients, in the presence of electric fields has been shown to result in rapid electrothermal flow.[32] In our attempt to understand the influence of the two components, that is, laser illumination and electric field, we first investigated the influence of laser illumination. The optically induced heating and resulting temperature profile was characterized by LIF thermometry. Intense illumination at 1064 nm ($\sim$10^6 W/cm^2) can cause localized heating of the ITO substrate, resulting in gradients of temperature and consequently in the electrical conductivity (σ) and permittivity (ε) of the fluid. Figure 4 presents the two-dimensional scalar temperature field created by laser heating at the bottom ITO coverslip. As expected, heating due to a single focused laser spot (Figure 2a) was axisymmetric with the temperature profile decreasing with radial distance (r) from the center of laser illumination. Temperature profiles as a function of radial distance from the center of the laser spot and peak temperatures
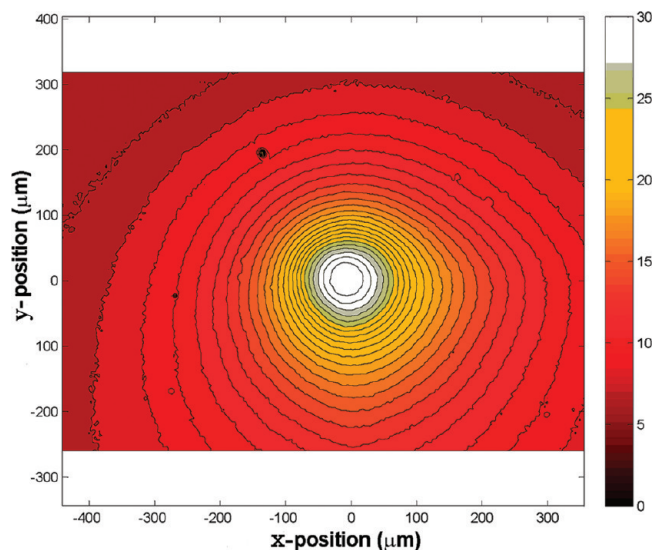
Figure 4. Measured temperature increase (°C) on the surface of an ITO coverslip with a laser power of 150 mW. The origin (0,0) refers to the center of laser focus.
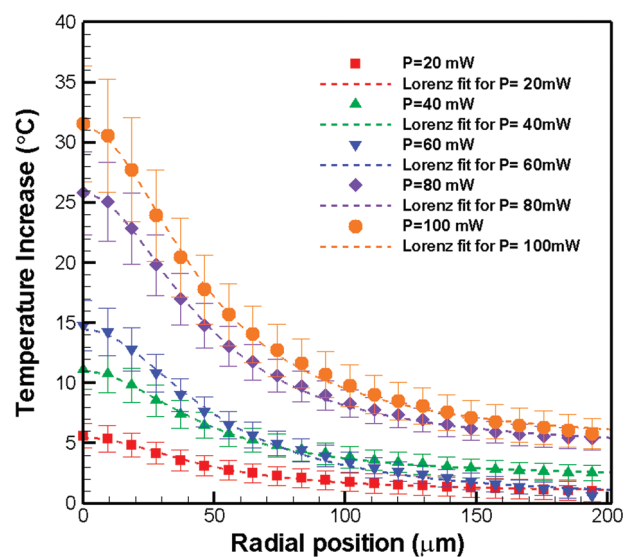
Figure 5. Temperature profiles measured from the center of laser illumination as a function of laser power.

were investigated (Figures 5 and 6). Error bars represent a total of two standard deviations. The temperature profiles were fitted with the Lorenz peak function of the form $T = T_0 + a(b/4r^2 + b^2)$, with a and b being fitting parameters (Figure 5). For a 20 mW applied laser power, the maximum temperature increase is $\sim$5 °C. When ITO substrates were replaced with plain glass substrates, the temperature increased only slightly (Figure 6), indicating that heating of the ITO is the dominant mechanism for the temperature increase. For all the above cases, no electric field was applied so that heating solely due to laser heating could be characterized.

The above results show that even though the absolute change in temperature might be small, the focused laser beam establishes a high-temperature gradient field. These gradients in the presence of an electric field can generate strong fluidic body forces, and from an earlier characterization of electrothermal fluid flow in such a setup[25] we know that fluid drag is expected to transport particles toward the illuminated region. While a higher laser power implies a larger temperature gradient and hence a higher magnitude of electrothermal fluid velocity, the AC electric field

(30) Williams, S. J.; Chamarthy, P.; Wereley, S. T. *J. Fluids Eng.* **2010**, *132*(2), 021103.

(31) Nadal, F.; Argoul, F.; Hanusse, P.; Pouligny, B.; Ajdari, A. Electrically induced interactions between colloidal particles in the vicinity of a conducting plane. *Phys. Rev. E* **2002**, *65* (6), 061409.

(32) Green, N. G.; Ramos, A.; Gonzalez, A.; Castellanos, A.; Morgan, H. Electric field induced fluid flow on microelectrodes: the effect of illumination. *J. Phys. D: Appl. Phys.* **2000**, *33* (2), L13−L17.
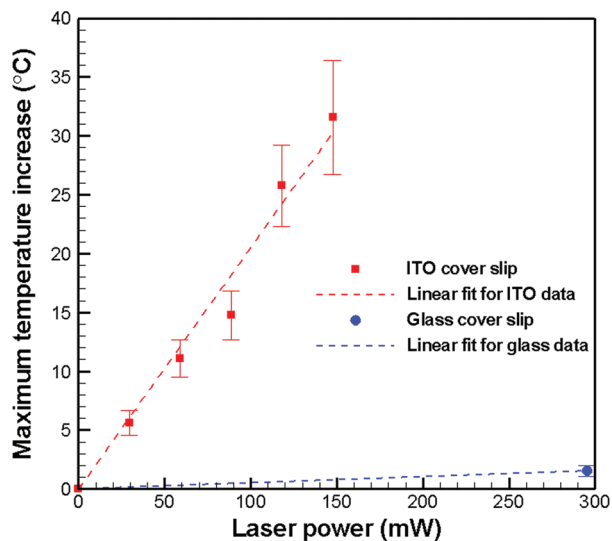
Figure 6. Maximum temperature increase on different substrates as a function of applied laser power.
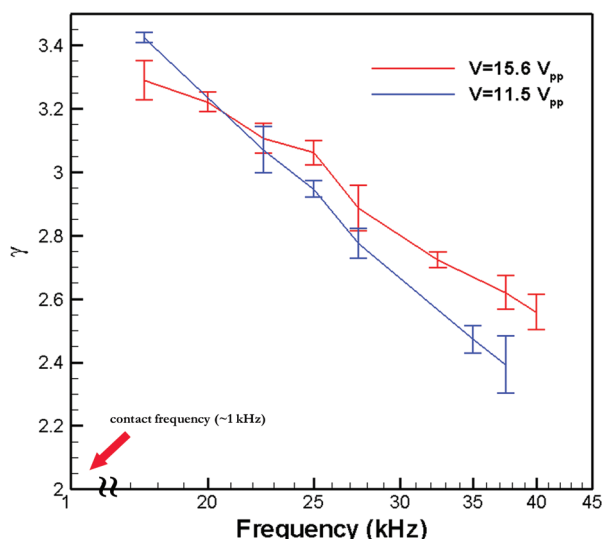
Figure 7. Ensemble averaged interparticle distance for a REP aggregation of 1.0 μm particles. This distance is function of AC frequency. The left arrow denotes the global "contact frequency", which was measured to be less than 1 kHz. The critical frequency, which is a frequency above which REP clusters become unstable, lies toward the right of the graphs.

also determines the magnitude of different forces acting on the particles. As a consequence, the REP aggregation of the form seen in Figure 2b is strongly dependent on the AC electric field, with the AC frequency being an important parameter. This dependence on AC frequency is reflected in the decrease of the ensemble averaged interparticle distance, γ (defined in eq 1), of the cluster, with an increase in AC frequency (Figure 7). However, the increase in AC frequency can only be continued until a critical AC frequency is reached. We define critical AC frequency (f_c) as the lowest AC frequency above which REP clusters cannot be maintained. This phenomenon will be elaborated upon later in this section.

In our attempt to understand the influence of the electric field on the aggregation, we observed that while activating the laser causes rapid particle transport to the illuminated site, deactivating the laser causes the particle group to scatter (Figure 8). The scattering behavior indicates the presence of particle–particle
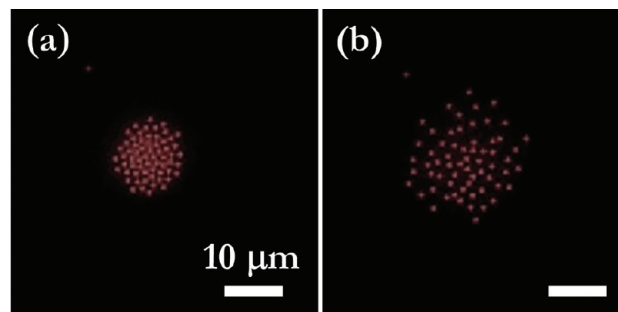

Figure 8. (a) REP cluster of 1.0 μm particles. Experimental conditions were an applied AC voltage of 13.1 V_{pp}, AC frequency of 20 kHz, and a laser power of 20 mW. (b) The cluster at $t \approx 2$ s after the laser is deactivated. As the dipoles (particles) are lined up side-by-side, there is a net repulsion force on the particles. These repulsive forces cause the particle cluster to disperse, thus showing that fluid drag due to the electrothermal microvortex provides the dominant force holding the cluster together.

repulsive forces, and a variation of these repulsive forces with the electric field will influence the scattering dynamics. To investigate the scattering dynamics, a REP induced cluster of 1.0 μm particles is initially created and then the illumination is deactivated and then the scattering is studied using high-speed video microscopy. Supporting Information shows the behavior of REP cluster due to deactivation/activation of the laser. Prior to investigating the effect of electric field on such scattering, we study the effect of the number of particles in the REP clump on particle repulsion (Figure 9). Scattering of the cluster was quantified by the increase in ensemble averaged interparticle distance, γ, as a function of time after the laser is deactivated. A direct consequence of this result is that comparison between scattering behaviors of REP clusters, at different parameter values, can be made even if they do not contain the same number of particles. Moreover, γ achieves an equilibrium value, of a few particle diameters, in less than 5 s. The asymptotic behavior of γ is well described by an exponential decay of the form $\gamma = \gamma_0 + c(1 - e^{-dt})$, with c and d being fitting parameters and t being time measured from the instant the laser is deactivated (Figure 9b). Ensemble averaging reduces the inherent stochastic component of dynamics at such small length scales and allows the repulsive dynamics to be well described by exponential curve fits. Physically, γ_0 can be identified with the ensemble averaged interparticle distance when the laser is still activated. The rate of increase of the ensemble averaged interparticle distance, γ, depends on the frequency and magnitude of the AC electric field (Figures 10 and 11). The dependence of the scattering dynamics on the electric field demonstrates that the repulsive forces governing the scattering behavior are AC electrokinetic in nature. This can be further verified by observing the behavior of a REP aggregation, when the electric field and laser are both simultaneously deactivated. In such circumstances, no dominant scattering behavior was observed and instead a very slow diffusive behavior was seen. Measurements could not be performed under such circumstances as particles diffused out of the viewing plane. Thus, the scattering behavior between the particles is noticeable only when the electric field is left activated. The scattering behavior, when the electric field is still activated, can be expected as the particles act as dipoles and dipole–dipole interaction in the present case is repulsive in nature.

Particle scattering experiments could only be carried out in the frequency window between the two extreme regions of Figure 7. At too low AC frequencies (close to "contact frequency"), attractive forces independent of the electrothermal drag dominate over the repulsive forces. On the other hand, at a high enough
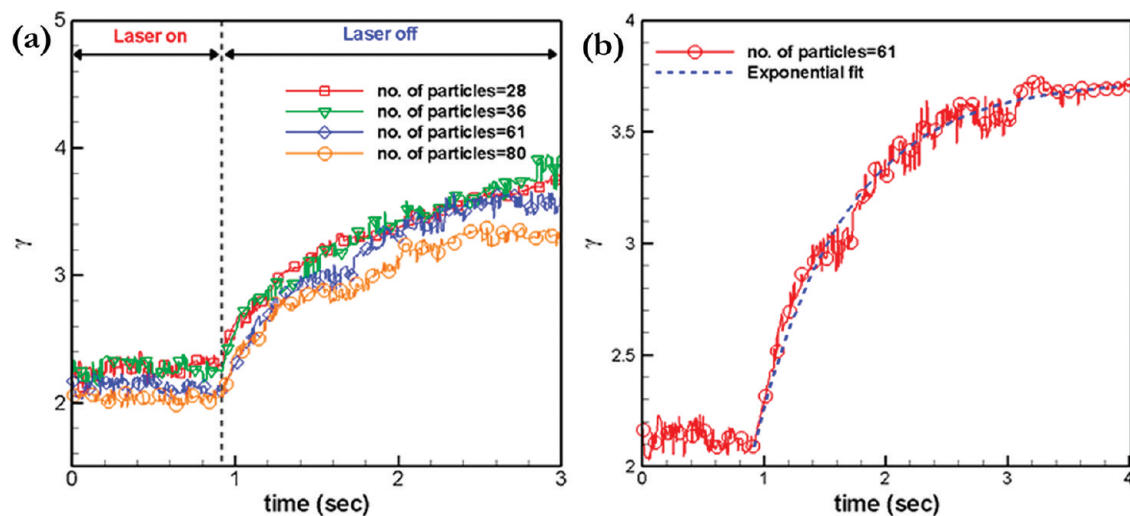
Figure 9. (a) Scattering of a REP aggregation of 1.0 μm polystyrene particles due to deactivation of laser results in an increase in the ensemble averaged interparticle distance. The clusters had a varying number of particles. The rate of increase of this distance does not depend on the number of particles initially in the clump. Thus, the magnitude of the total repulsive force on a single particle is independent of the number of particles in the clump, which signifies that the repulsive forces decay strongly with distance. Experimental conditions were $V = 11.2$ V_{pp}, $f = 27.5$ kHz, and initial $P = 20$ mW. (b) Exponential decay fit to experimental data. The exponential decay function describes the data well (typical $R^2 > 0.95$).
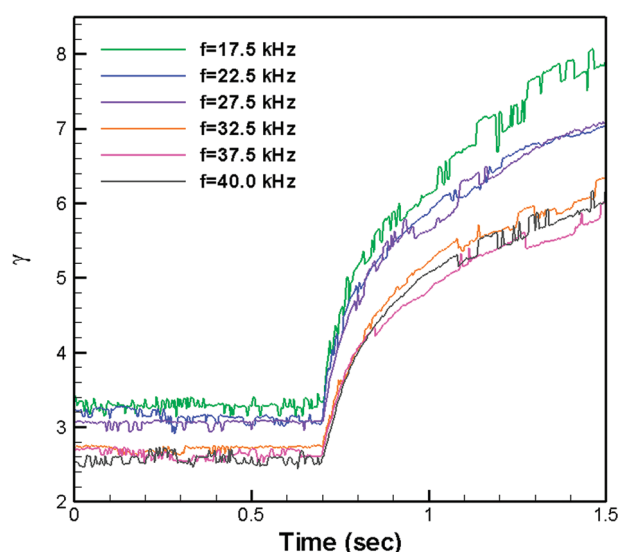
**Figure 10.** Scattering of a REP aggregation of 1.0 μm particles due to deactivation of laser as a function of applied AC frequency. The variation in the rate of scattering of the particles with AC frequency suggests that the induced dipole moment varies with AC frequency. Such a variation can be expected due to nonequilibrium EDL polarization. Experimental conditions were $V = 15.6$ V_{pp} and initial $P = 20$ mW (6 out of 8 cases shown for clarity). Exponential decay fits for experimental data have not been displayed for clarity.
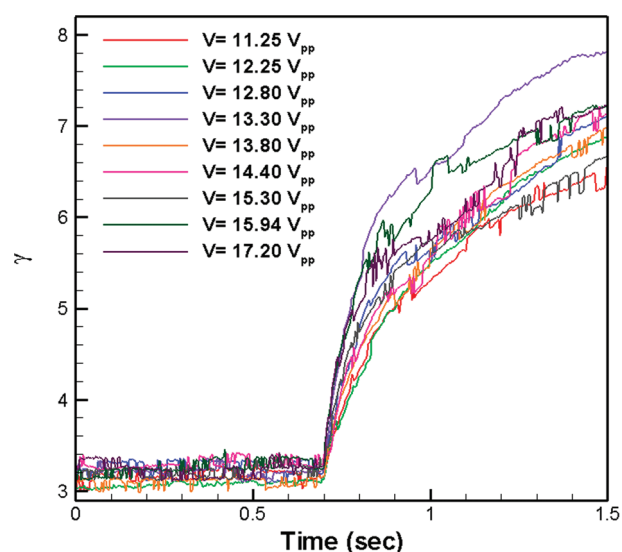
**Figure 11.** Scattering of a REP aggregation of 1.0 μm polystyrene particles due to deactivation of laser as a function of applied AC voltage. Experimental conditions were $f = 19.6$ kHz and initial $P = 20$ mW (9 out of 11 cases shown for clarity). Exponential decay fits for experimental data have not been displayed for clarity.

frequency (close to critical frequency, f_c), the REP cluster becomes unstable. To illustrate this onset of instability at a high enough AC frequency, we assembled a REP cluster of 1.0 μm beads at a frequency of 15 kHz and then increased the AC frequency. We found that close to a certain AC frequency the REP cluster becomes unstable and a decrease in the number of particles is observed (Figure 12). As the AC frequency is further increased, REP-based aggregation is no longer observed. Particles are still transported by the electrothermal microvortex, but they no longer collect on the electrode surface. This behavior demon-

strates the existence of a threshold or critical frequency related to the process. Thus, at $f \approx f_c$, the REP cluster becomes unstable and aggregated particles are carried away into the bulk by the electrothermal microvortex. This phenomenon is shown in the Supporting Information. This situation is illustrated in Figure 13, where the competition between the vertical or normal particle−electrode interaction force and drag force by the electrothermal microvortex causes the threshold phenomenon. At the critical frequency, the particle−electrode interaction force is overcome by the fluid drag, that is, $F_{\text{drag}-\text{ET}}^{\text{normal}} > F_{\text{particle}-\text{electrode}}^{\text{normal}}$, and particles are transported into the bulk medium. Thus, the existence of the critical AC frequency is a direct consequence of the frequency dependence of both the vertical particle−electrode forces and the electrothermal microvortex. Figure 14 shows the experimentally
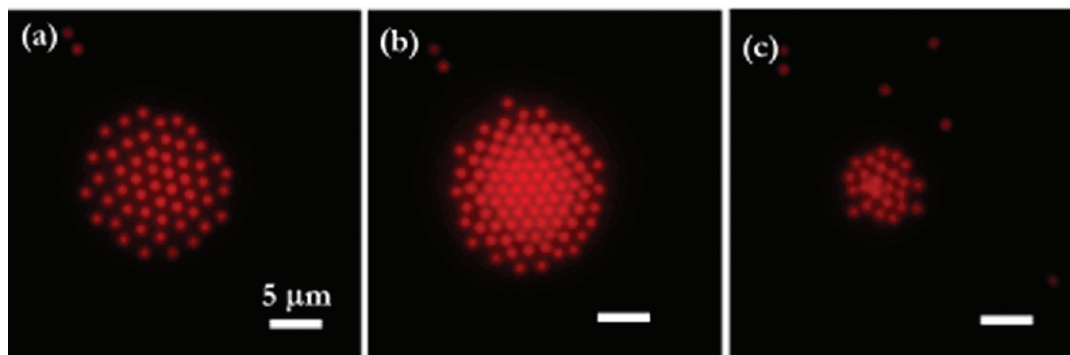
Figure 12. Stability of a REP aggregation of 1.0 μm particles is a function of the applied AC frequency: (a) cluster of 1.0 μm particles at f = 10 kHz and (b) f = 30 kHz, and (c) REP cluster close to its critical frequency (f = 40 kHz). The size of the cluster has significantly diminished. Applied AC voltage and laser power were maintained at 10.5 V_{pp} and 20 mW, respectively.
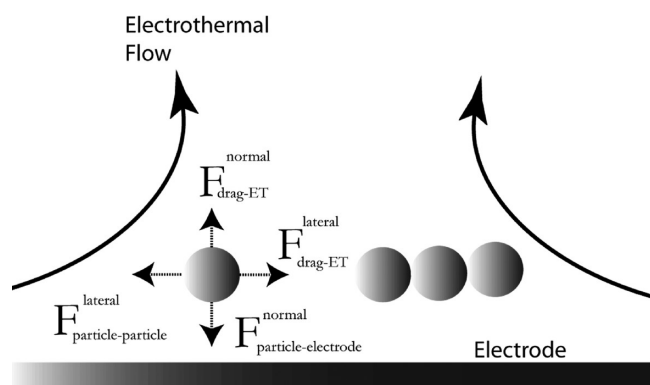
Figure 13. Various forces on a particle in the REP cluster. $F_{drag-ET}^{normal}$, $F_{drag-ET}^{lateral}$ denote the drag forces exerted by the electrothermal flow on the particle. $F_{particle-electrode}^{normal}$ denotes the attractive force exerted by the electrode on the particle. $F_{particle-particle}^{lateral}$ denotes net the repulsive force exerted on a particle by other particles, when only the electric field is activated.
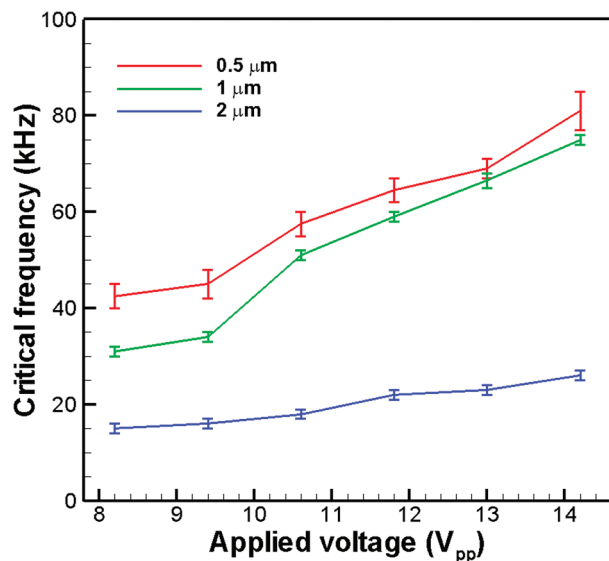
Figure 14. Variation of critical AC frequency with AC voltage for carboxylate-modified polystyrene particles of varying diameters. An applied laser power of 20 mW was used.

measured critical frequencies for three different particle diameters. The critical frequency was visually measured for each bead size. For each observation, two measurements were made: the lowest frequency at which a stable REP cluster became

unstable and the highest frequency at which no REP aggregation was observed. Each interval in Figure 14 shows this range. As can be seen for all three particle diameters, the critical frequency increases with AC voltage. The critical frequency exhibits a linear dependence on the applied electric field strength ($f_c \sim |\mathbf{E}|$) and is also particle diameter dependent. For similar particles (carboxylate-modified polystyrene particles), Figure 14 shows that the critical frequency is largest for the smallest particle. For 0.1 μm particles, also the threshold behavior was seen, and although individual particles could not be distinguished, the aggregation was quantified indirectly through fluorescent emission (Figure 15). Figure 15b shows that the intensity of the REP aggregation of 0.1 μm particles decreases with increasing AC frequency and finally becomes indistinguishable from the background, indicating reaching of the critical frequency. From visual observation, the critical frequency for the REP aggregation under conditions of Figure 15 was observed to be ~75 kHz.

4. Discussion

Electrothermal Flows. We have seen that aggregation does not result from the sole application of laser illumination. Hence, thermophoretic migration[33] was not significant in our setup. While laser heating can result in convective flows, the convective fluid velocity scale in our setup was at least an order of magnitude smaller than the electrothermal fluid velocity scale.

Interaction of laser illumination with a fluid medium can occur through laser heating, which can lead to temperature gradients within a fluid (Figures 4−6), and these gradients in turn can produce gradients in density, electrical conductivity, and electrical permittivity. While density gradients can lead to fluid flow through natural convection, gradients in electrical conductivity and electrical permittivity of the fluid in the presence of electric fields can generate electrothermal flow.[34] However, a comparative analysis of different forces in microsystems shows that the buoyancy forces are relatively unimportant when electrical forces are present.[1] This explains the experimental observation of no aggregation under the sole influence of laser illumination. Thus, the role of convective flows in the presence of electrothermal flows can be neglected. The dependence of the time averaged electrothermal body force ($\langle \mathbf{g} \rangle$) on the gradient of the temperature field

(33) Duhr, S.; Braun, D. Why molecules move along a temperature gradient. *Proc. Natl. Acad. Sci. U.S.A.* **2006**, *103* (52), 19678−19682.
(34) Ramos, A.; Morgan, H.; Green, N. G.; Castellanos, A. Ac electrokinetics: a review of forces in microelectrode structures. *J. Phys. D: Appl. Phys.* **1998**, *31*, (18), 2338−2353.
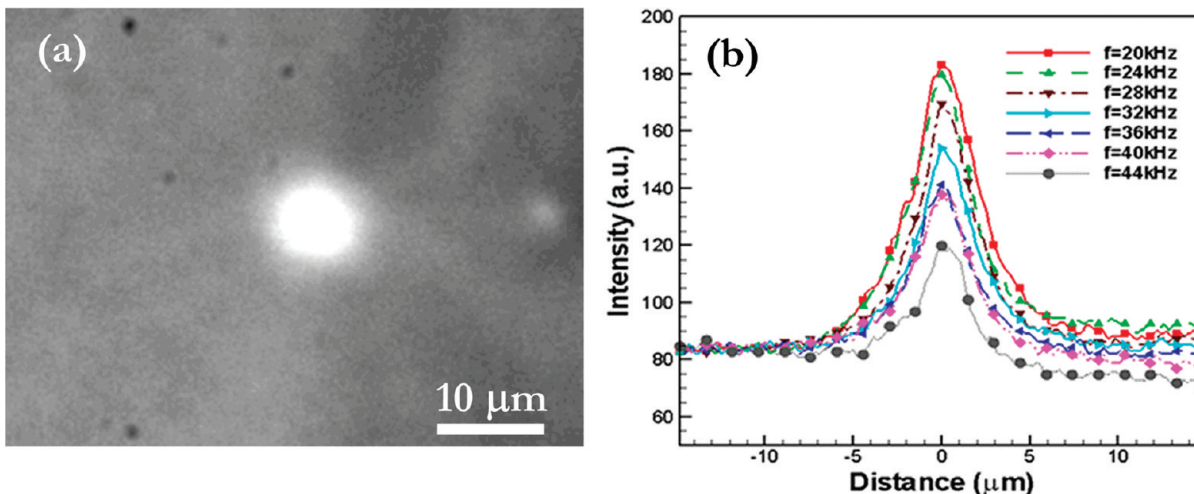
Figure 15. (a) REP generated accumulation of 0.1 μm polystyrene particles on the bottom ITO surface with an applied 13.5 V_{pp} AC voltage, 20 kHz AC frequency, and 20 mW laser power. Individual particles cannot be discerned at these scales with epifluorescent microscopy, and particle aggregation is represented by a "glowing" clump. (b) Fluorescent intensity profiles of a 0.1 μm bead cluster as a function of AC frequency. The applied AC voltage was 13.5 V_{pp}, and laser power was 20 mW. The existence of a critical frequency observed previously for larger particle diameters can also be seen for 0.1 μm particles.

(∇T) and electric field is given by[35]

$$\langle \mathbf{g} \rangle = \frac{1}{2} Re \left(\frac{\sigma \varepsilon (\alpha - \beta)}{\sigma + i\omega\varepsilon} (\nabla T \cdot \mathbf{E}) \mathbf{E}^* - \frac{1}{2} \varepsilon\alpha |\mathbf{E}|^2 \nabla T \right) \quad (2)$$

where $Re(...)$ denotes the real part of the expression, $\mathbf{E}$ is the electric field vector, $\mathbf{E}^*$ is the complex conjugate of the electric field vector, ω is the angular frequency of the applied electric field, and β and α are the fractional changes of σ and ε with temperature given by $1/\sigma(d\sigma/dT)$ and $1/\varepsilon(d\varepsilon/dT)$, respectively. In REP, we assume that the thermal field is generated by the laser and neglect Joule heating, so that the electrothermal body force scales as the second power of the electric field ($\langle \mathbf{g} \rangle \sim |\mathbf{E}|^2$). The body force is also frequency dependent but can be assumed to be constant for the regime of operation of REP, since we typically operate well below the charge relaxation frequency of the liquid electrolyte (Figure 16).

Particle Scattering Measurements. Any behavior in REP needs to be understood in terms of three components: (i) colloidal forces which are independent of the applied electric field, (ii) purely electrokinetic forces which are independent of laser illumination, and (iii) electrothermal flows. Colloidal forces result from interplay between van der Waals forces and the electrostatic double layer interaction, and these can be expected to be present in any colloidal system independent of any applied electric field. Such colloidal forces might be understood in terms of the classical theory of Derjaguin, Landau, Verwey, and Overbeek (DLVO).[36,37] Purely electrokinetic forces independent of any laser illumination can result from phenomena such as induced dipole interactions,[1] induced-charge electro-osmosis,[38,39] nonequilibrium
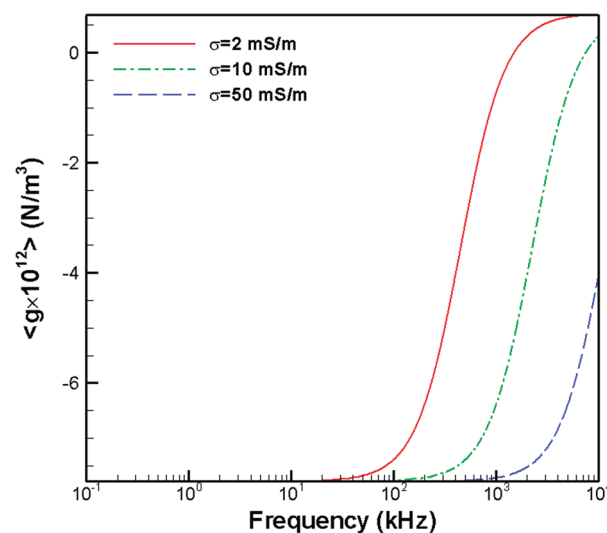
Figure 16. Variation of the electrothermal body force with frequency for different medium conductivities, unit temperature gradient, and electrical field strength. These curves were calculated from eq 2.

surface phenomena,[40] and electrohydrodynamic flows.[41] Electrothermal flows have already been discussed in the previous section. "Global aggregations" and scattering experiments are caused by colloidal and purely electrokinetic forces. REP and the thresholding behavior in REP are caused by all the three colloidal, purely electrokinetic, and electrothermal forces.

Our particle scattering experiments (Figures 9−11) can provide insight into the characteristics of the forces present in REP. To understand how the scattering experiments can lead to force measurement, we consider that for a colloidal particle moving under the influence of a force field $\mathbf{F}(\mathbf{x})$, its trajectory is given by

$$\xi \frac{d\mathbf{x}}{dt} = \mathbf{F}(\mathbf{x}) \quad (3)$$

(35) Green, N. G.; Ramos, A.; Gonzalez, A.; Castellanos, A.; Morgan, H. Electrothermally induced fluid flow on microelectrodes. *J. Electrost.* **2001**, *53* (2), 71−87.
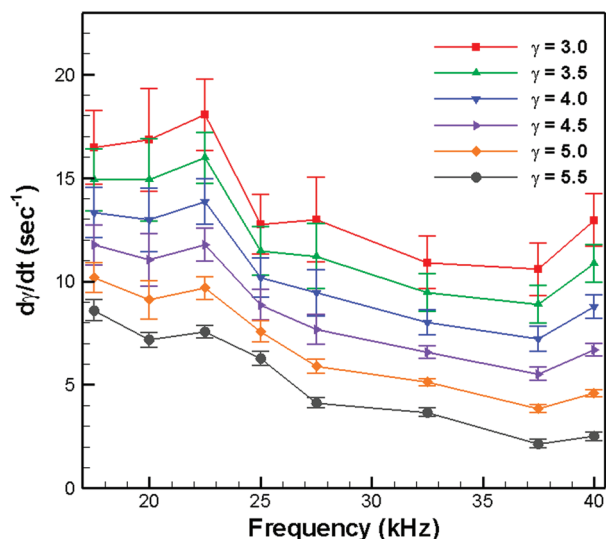
(36) Verwey, E. J.; Overbeek, J. T. G. *Theory of stability of lyophobic colloids*; Elsevier: Amsterdam, 1948.

(37) Derjaguin, B. V.; Landau, L. Theory of the stability of strongly charged lyophobic sols and the adhesion of strongly charged particles in solutions of electrolytes. *Acta Physicochim. URSS* **1941**, *14*, 633.

(38) Bazant, M. Z.; Squires, T. M., Induced-charge electrokinetic phenomena: Theory and microfluidic applications. *Phys. Rev. Lett.* **2004**, *92* (6), 066101.

(39) Squires, T. M.; Bazant, M. Z. Induced-charge electro-osmosis. *J. Fluid Mech.* **2004**, *509*, 217−252.

(40) Dukhin, S. S. Nonequilibrium electric surface phenomena. *Adv. Colloid Interface Sci.* **1993**, *44*, 1−134.

(41) Ristenpart, W. D.; Aksay, I. A.; Saville, D. A. Assembly of colloidal aggregates by electrohydrodynamic flow: Kinetic experiments and scaling analysis. *Phys. Rev. E* **2004**, *69* (2), 021405.

Figure 17. Scattering dynamics of the 1.0 μm particles were analyzed to yield dγ/dt values for different AC frequencies. The exponential fits to the experimental data (Figure 10) yielded fitting parameters with 95% confidence intervals, and these fits were used to calculate dγ/dt values. dγ/dt corresponds to the average repulsive force.

Figure 18. dγ/dt as a function of γ for different AC frequencies. This figure corresponds to experimental data shown in Figure 10. A linear dependence of dγ/dt on γ is a consequence of the exponential decay behavior.

where ξ is the particle's viscous drag coefficient. Generalizing from eq 3, one can see that, for the scattering experiments, the ensemble averaged repulsive force is proportional to dγ/dt. Now, for scales typical of microsystems, heat transfer through thermal diffusion typically dominates over convection driven heat transfer.[1] Recall that the laser power used for the scattering experiments was only 20 mW, and this laser power only causes a maximum temperature of ~5 °C. As such, for the particular system used here, a simple heat-transfer analysis shows that deactivation of the laser would lead the system to reach thermal equilibrium within ~10^{-3} s. As the data acquisition rate for the particle scattering experiments was only 250 fps, the deactivation of the laser can be considered to result in an instantaneous termination of the electrothermal hydrodynamic drag. As the drag from the electrothermal vortex vanishes, the net repulsive particle–particle interaction forces (Figure 13) lead to an increase in the ensemble averaged interparticle distance. This net repulsive force ($F_{particle-particle}^{lateral}$) is proportional to d$\gamma$/d$t$ and is composed of colloidal and purely electrokinetic forces.

Data processing from the scattering experiments, of 1.0 μm particles, reveals that dγ/dt is AC frequency dependent (Figure 17). The absolute decrease in dγ/dt can differ from 20 to 70% (depending on γ) as the AC frequency is increased from 17.5 to 40 kHz. This decreasing trend is approximately linear. Moreover, dγ/dt decreases linearly with distance (γ) (Figure 18). This behavior is a direct consequence of the exponential decay behavior of γ. Scattering experiments of 1.0 μm particles at different AC voltages (Figure 11), also indicate that dγ/dt depends on AC voltage (Figure 19). While dγ/dt does not display a monotonically increasing trend with AC voltage, the trend can still be described as increasing. In fact, dγ/dt changes by more than 100% with a voltage increase from 11.25 to 17.2 V_{pp}. This dependence of dγ/dt on the electric field results the purely electrokinetic component of the repulsive force.

At this point, consideration should be given to the nature of this purely electrokinetic component of the repulsive force. We have seen before that in the present experimental setup that "global aggregation" in the absence of any laser illumination was observed for $f < 1$ kHz, but for $f \geq 2$ kHz, the particle aggregation
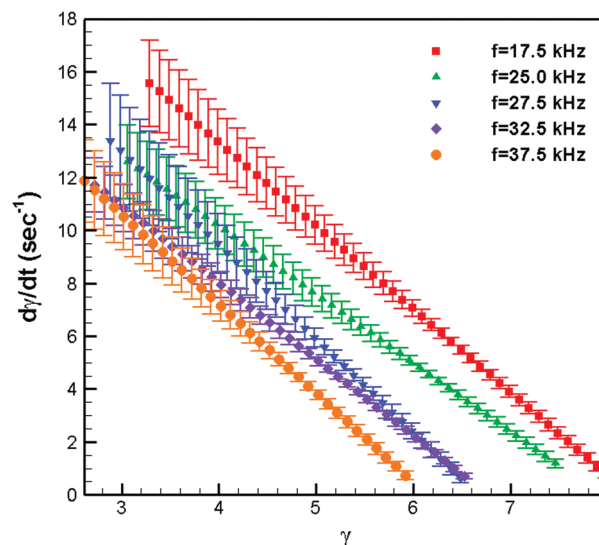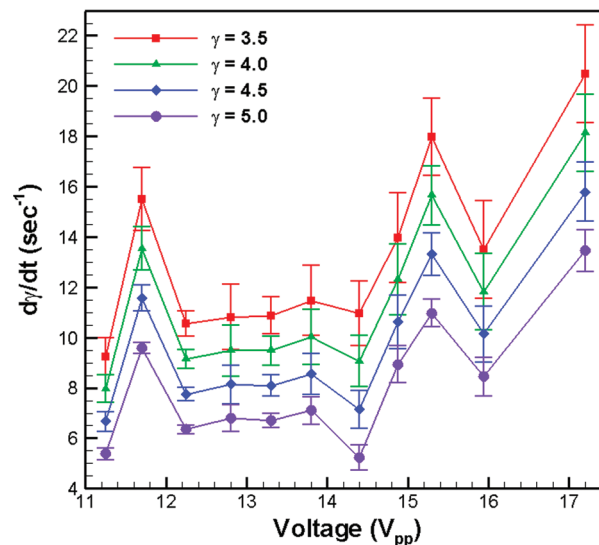
Figure 19. Scattering dynamics of the 1.0 μm particles were analyzed to yield dγ/dt values for different AC voltages. The exponential fits to the experimental data (Figure 11) yielded fitting parameters with 95% confidence intervals, and these fits were used to calculate dγ/dt values.

ceased. Aggregations of such nature have been studied extensively and explained through various theories.[10–12,41–43] For low conductivity aqueous solutions such as those used in the present investigation, clustering is often understood in terms of an attractive drag from electrohydrodynamic (EHD) flows and repulsive forces from dipole–dipole interactions. Note that the conventional Maxwell–Wagner interfacial polarization,[1] which is often used to understand induced dipole moments, does not predict any change in the dipole moment of the particles with AC frequency, since in REP we operate far below the

(42) Ristenpart, W. D.; Aksay, I. A.; Saville, D. A. Electrically guided assembly of planar superlattices in binary colloidal suspensions. *Phys. Rev. Lett.* **2003**, *90* (12), 128303.

(43) Solomentsev, Y.; Bohmer, M.; Anderson, J. L. Particle clustering and pattern formation during electrophoretic deposition: A hydrodynamic model. *Langmuir* **1997**, *13* (23), 6058–6068.
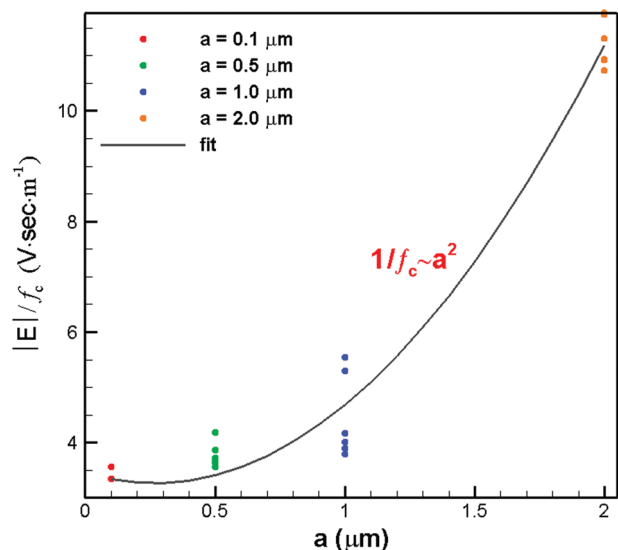
Figure 20. The critical frequency displays an inversed squared dependence on particle diameter.

Maxwell–Wagner relaxation frequency. Ristenpart et al.[41] predicted that EHD forces cause such aggregation and that these forces scale with the square of the electric field ($\sim |\mathbf{E}|^2$) and the inverse of the AC frequency ($\sim 1/f$). Since for $f \geq 2$ kHz in the present investigation "global aggregation" ceased, one can conclude that EHD forces alone are unable to overcome the repulsive dipole–dipole forces. In this regime ($f \geq 2$ kHz), the attractive EHD forces would also be expected to decrease as AC frequency increases. If the dipole forces were to remain constant, at higher frequencies ($f \geq 15$ kHz), the net repulsive force can be expected to increase with frequency due to decrease in the EHD forces. However, particle scattering experiments with REP indicate that the $F_{particle-particle}^{lateral}$ actually decreases when the AC frequency is increased to 17.5 kHz from 40 kHz (Figure 17). This anomaly suggests the presence of another relaxation phenomenon, other than the relaxation of the EHD flow. A possible explanation lies in the frequency dependent dipole moment resulting from nonequilibrium phenomenon.[40] This phenomenon arises from the polarization of the electrical double layer (EDL), around a particle, in the presence of an external applied electric field.[44–50] Thus, the net dipole moment of particles is this present AC frequency regime can be considered to arise from a combination of the Maxwell–Wagner interfacial polarization and nonequilibrium EDL polarization.

If the dipole moment indeed decreases, a similar decrease (with AC frequency) in the vertical particle–electrode interaction forces resulting from the effect of image charges can also be expected. With increasing AC frequency in a REP aggregation, it can be expected that the vertical drag from the vortex may eventually exceed the particle–electrode attractive forces. Such

a decrease would account for the existence of a critical frequency in REP. Moreover, the relaxation mechanism associated with the EDL polarization process has an associated relaxation frequency (f_{EDL}) that scales as the square of the particle diameter ($f_{EDL} \sim 1/a^2$).[1,50] Figure 20 shows that the inverse of the scaled critical frequency displays a squared dependence on the particle diameter $f_c \sim 1/a^2$. Thus, the particle scattering experiments and critical frequency measurements indicate the participation of the nonequilibrium EDL polarization phenomenon.

The variation of the net repulsive force with the applied electric field strength is not totally understood (Figure 19), but the measured force approximately has a second-order polynomial dependence on the electric field strength. The coefficient values indicate a substantial linear dependence of this fit. Future experiments will further explore this behavior, including characterizing the particle–electrode electrokinetic forces as a function of applied voltage and medium conductivity. The preliminary results presented here have established the existence of a relaxation phenomenon.

REP and Other Opto-Electric Techniques. The REP technique belongs to the broader category of opto-electric particle manipulation techniques. Another separate, dynamic opto-electric technique was introduced by Chiou et al., and it is termed opto-electronic tweezers (OET). While both REP and OET are opto-electric techniques, they differ not only in implementation but also in the underlying physics. In a typical OET setup, the two substrates are biased with an AC electric field and one of the substrates in OET is coated with hydrogenated amorphous silicon (a:Si–H), which is a strong photoconductor.[51,52] The use of a strong photoconductor such as a:Si–H allows an OET device to use far lower optical densities compared to REP.[53] Also, in OET, an illuminated region can be regarded as a "virtual electrode", and thus, an OET device can handle particles with dielectrophoresis or a combination of light-actuated AC electro-osmosis and electrothermal flows.[54]

5. Conclusions

REP is a novel particle manipulation and concentration technique, which can concentrate colloidal particles at user-defined locations on an electrode surface. The participation of an electrothermal microvortex in the aggregation process induces bulk particle transport, making REP an effective technique for dynamic manipulation. The use of optical techniques bestows active control over the placement of colloidal aggregations as well as enabling various operations such as translation of assembled structures. Trapping in REP is essentially two-dimensional in nature, as particle clusters can only be assembled over an electrode surface. The technique can efficiently pattern and trap particles ranging in size from 50 nm to 3.0 μm.

In this paper, we have expanded upon the initial disclosure of REP. We have systematically explored the various aspects of REP, including the heating caused by laser illumination and the nature of the forces in colloidal aggregation. The large number of physical forces make REP a complex process. Hence, some simplifications, such as restrictions on the optical landscape, were

(44) Fixman, M. Thin double-layer approximation for electrophoresis and dielectric response. *J. Chem. Phys.* **1983**, *78* (3), 1483–1491.

(45) Green, N. G.; Morgan, H. Dielectrophoresis of submicrometer latex spheres. 1. Experimental results. *J. Phys. Chem. B* **1999**, *103* (1), 41–50.

(46) Lyklema, J.; Leeuwen, H. P. v.; Vliet, M. v.; Cazabat, A. M. *Fundamentals of interface and colloid science*; Academic Press: London, San Diego, 1991; p v.

(47) O'Konski, C. T. Electric properties of macromolecules V: theory of ionic polarization in polyelectrolytes. *J. Phys. Chem.* **1960**, *64*, 605–619.

(48) Schurr, J. M. On theory of dielectric dispersion of spherical colloidal particles in electrolyte solution. *J. Phys. Chem.* **1964**, *68* (9) 2407.

(49) Schwan, H. P.; Schwarz, G.; Maczuk, J.; Pauly, H. On low-frequency dielectric dispersion of colloidal particles in electrolyte solution. *J. Phys. Chem.* **1962**, *66* (12), 2626.

(50) Schwarz, G. A theory of low-frequency dielectric dispersion of colloidal particles in electrolyte solution. *J. Phys. Chem.* **1962**, *66* (12), 2636.

(51) Chiou, P. Y.; Ohta, A. T.; Wu, M. C. Massively parallel manipulation of single cells and microparticles using optical images. *Nature* **2005**, *436* (7049), 370–372.

(52) Hwang, H.; Park, J. K. Rapid and selective concentration of microparticles in an optoelectrofluidic platform. *Lab Chip* **2009**, *9* (2), 199–206.

(53) Jamshidi, A.; Neale, S. L.; Yu, K.; Pauzauskie, P. J.; Schuck, P. J.; Valley, J. K.; Hsu, H. Y.; Ohta, A. T.; Wu, M. C. NanoPen: Dynamic, low-power, and light-actuated patterning of nanoparticles. *Nano Lett.* **2009**, *9* (8), 2921–2925.

(54) Chiou, P. Y.; Ohta, A. T.; Jamshidi, A.; Hsu, H. Y.; Wu, M. C. Light-actuated ac electroosmosis for nanoparticle manipulation. *J. Microelectromech. Syst.* **2008**, *17* (3), 525–531.

necessary in order to have a better understanding. For example, the scattering of particles when a laser is deactivated is in essence an extreme high-dimensional dynamical system. A simplification was achieved by studying the behavior of the ensemble averaged interparticle distance as a function of other parameters. Another important conclusion of this work is the existence of a size dependent critical capturing frequency. This adds to the versatility of the technique, making possible the selective clustering of particles based on their sizes. We also show that the interparticle distance in an REP-based cluster can be tuned with AC frequency. Techniques to create tunable colloidal aggregations are being actively pursued by the scientific community.[55]

In summary, we have taken an important step in the characterization of the REP process. However, extensive research on theoretical modeling and experimental aspects are still necessary before a complete understanding of the technique can be gained. For example, particle dynamics in a REP trap are essentially stochastic in nature. Similar to the modeling of stochastic noise in an optical trap,[56,57] research needs to be directed at understanding the role of stochastic dynamics in the behavior of particles in a REP trap.

Supporting Information Available: Videos showing how the particle group responds to change in the experimental parameters. This material is available free of charge via the Internet at http://pubs.acs.org.

(55) Liu, Y.; Xie, R. G.; Liu, X. Y. Fine tuning of equilibrium distance of two-dimensional colloidal assembly under an alternating electric field. *Appl. Phys. Lett.* **2007**, *91* (6), 063105.

(56) Banerjee, A. G.; Balijepalli, A.; Gupta, S. K.; LeBrun, T. W., Generating Simplified Trapping Probability Models from Simulation of Optical Tweezers Systems. *ASME J. Comput. Inf. Sci. Eng.* **2009**, *9* (2), 021003.

(57) Tatarkova, S. A.; Sibbett, W.; Dholakia, K. Brownian particle in an optical potential of the washboard type. *Physical Review Letters* **2003**, *91* (3), 038101.